

See discussions, stats, and author profiles for this publication at: <https://www.researchgate.net/publication/51692900>

# Molecular Modeling of Hydrotalcite Structure Intercalated with Transition Metal Oxide Anions: CrO<sub>4</sub>2- and VO<sub>4</sub>3-

ARTICLE in THE JOURNAL OF PHYSICAL CHEMISTRY A · NOVEMBER 2011

Impact Factor: 2.69 · DOI: 10.1021/jp2079499 · Source: PubMed

---

CITATIONS

3

---

READS

108

## 4 AUTHORS, INCLUDING:



Vinuthaa Murthy

Charles Darwin University

11 PUBLICATIONS 30 CITATIONS

[SEE PROFILE](#)

# Molecular Modeling of Hydrotalcite Structure Intercalated with Transition Metal Oxide Anions: $\text{CrO}_4^{2-}$ and $\text{VO}_4^{3-}$

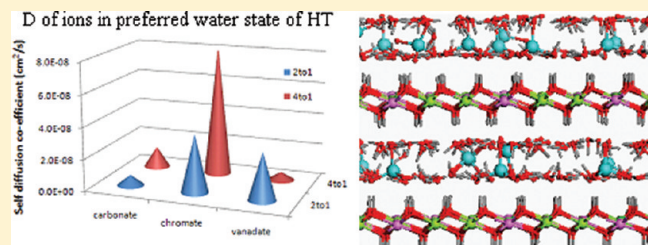
Vinuthaa Murthy,<sup>\*,†</sup> Howard D. Smith,<sup>‡</sup> Hong Zhang,<sup>§</sup> and Sean C. Smith<sup>§</sup>

<sup>†</sup>School of Environmental and Life Sciences, Charles Darwin University, Darwin, NT 0909, Australia.

<sup>‡</sup>Mining and Major Projects, Northern Land Council, Darwin, NT 0810, Australia

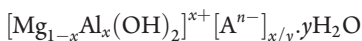
<sup>§</sup>Australian Institute for Bioengineering and Nanotechnology, The University of Queensland, Brisbane, Qld 4072, Australia

**ABSTRACT:** Molecular dynamics (MD) simulations are used to study the interlayer structure, hydrogen bonding, and energetics of hydration of Mg/Al (2:1 and 4:1) layered double hydroxide (LDH) or hydrotalcite (HT) intercalated with oxymetal anions,  $\text{CrO}_4^{2-}$ , and  $\text{VO}_4^{3-}$ . The ab initio forcefield COMPASS is employed for the simulations. The charge on the oxymetal anions is determined by quantum mechanical density functional theory. The structural behavior of the oxymetal anions in LDH directly relates to the energetic relationships, with electrostatic and H-bonding interactions between the anions, hydroxide sites of the metal hydroxide layers, and the interlayer water molecules. Distinct minima in the hydration energy indicate the presence of energetically well-defined structural states with specific water content. The experimentally identified variability in the retention of the  $\text{CrO}_4^{2-}$  and  $\text{VO}_4^{3-}$  is well reflected in the calculations and self-diffusion coefficients obtained from the simulations give insight into the mobility of the intercalated species.



## 1. INTRODUCTION

Synthetic Hydrotalcite having variable stoichiometry is readily formed by reaction between magnesium salts and sodium aluminate solution. It consists of octahedral layers of mixed magnesium and aluminum hydroxides, also known as layered double hydroxides (LDH), between which anionic compounds become intercalated, and has a general stoichiometry:



where A may be any anion. These anions may be exchanged with others if the hydrotalcite remains in solution for a long period.

Under dynamic industrial conditions, hydrotalcite-like materials having ratios of 2:1 and 4:1 dominate the precipitate.<sup>1</sup> Although  $\text{CO}_3^{2-}$  and  $\text{C}_2\text{O}_4^{2-}$  are the dominant intercalates, any larger in situ metalloids and transition metal molecules may also be recovered. Recovery of these anions is pH-dependent, primarily because of changes that occur to the molecular structure and charge density of hydrotalcite.<sup>1</sup> In situ transition metal anions may become incorporated into the hydrotalcite in a variety of ways. They may form coprecipitates, replace Mg or Al in the octahedral layers, bond as pillars joining these layers, surface adsorb, or intercalate between the octahedral layers. Each of these modes results in a different degree of stability of the hydrotalcite matrix and the ease by which the transition metal may be released back into the environment.

Reaction with seawater (which contains a high concentration of magnesium) has long been used by the alumina industry as a means of neutralizing its alkaline wastewater prior to disposal into the ocean, but even in a well-managed disposal system

recovery of the hydrotalcitic precipitate is never complete.<sup>2,3</sup> Molecular structure and stoichiometry depend upon the operating conditions under which the hydrotalcite is produced,<sup>4,5</sup> meaning that this precipitate may not be as stable as originally thought, and may in fact create a source of future environmental contamination. Some of the intercalated anions contained within hydrotalcite found on the seafloor around coastal alumina refineries may be environmentally detrimental, so it is of interest to develop a means of estimating the stability of hydrotalcite and the rate at which a specific intercalate might be released. Better understanding of the nature of hydrotalcite through modeling may provide an opportunity to identify and select operating conditions that allow both the recovery of specific toxic anions and the stability of the hydrotalcite matrix to be maximized.

Experimental techniques like PXRD, ATR, and FTIR<sup>5,6</sup> have been used to characterize the structure of the hydrotalcite, but disordering within the poorly crystalline hydrotalcite particles makes it difficult to fully elucidate interlayer arrangement of the intercalated anions and water molecules. However, details of the interlamellar properties of hydrotalcite that are difficult to interpret from experimentation can be estimated through the use of computational chemistry tools based on classical force fields and quantum-chemical methods of electronic structure calculations and the structure and dynamics of these layered double hydroxides evaluated on an atomic scale.

**Received:** August 18, 2011

**Revised:** October 4, 2011

Over the past decade, a number of molecular models of hydrotalcite have been prepared, leading to improved insight of its interlamellar structure and dynamics.<sup>7–13</sup> This includes a better understanding of hydration and swelling,<sup>14,15</sup> bonding,<sup>16,17</sup> and diffusivity of intercalated anions.<sup>18</sup> Although these models have considered a range of anions from simple  $\text{Cl}^-$ ,  $\text{CO}_3^{2-}$ , and  $\text{NO}_3^-$ <sup>19</sup> to large or complicated organic anions,<sup>20</sup> modeling of intercalated transition metal anions has yet to be seriously undertaken. This paper attempts to partly address this knowledge gap by comparing a number of measurable modeled parameters generated using computational molecular dynamics (MD) simulations for two transition metal anions ( $\text{CrO}_4^{2-}$  and  $\text{VO}_4^{3-}$ ) with those for  $\text{CO}_3^{2-}$ , one of the most thermodynamically stable intercalates.

## 2. METHODS

**2.1. Experimental.** The 1 molar sodium aluminate solutions were prepared by dissolution of aluminum pellets or foil in sodium hydroxide. The solutions were cooled and filtered to remove any residue prior to final dilution and standardization. Sodium salts of vanadate, chromate, and carbonate were dissolved and added directly into the sodium aluminate immediately prior to reaction with 1 molar magnesium chloride. Varying relative volumes of each solution allowed production of synthetic hydrotalcite containing transition metal concentrations comparable to those expected in the industrial seawater neutralization system.

Stability of the anion within the interlamellar space is an important parameter that defines its capability as an environmental ameliorant. If the anions are not firmly bonded, they may be exchanged by other more thermodynamically stable anions such as  $\text{CO}_3^{2-}$  and the material's usefulness diminished. To gain an insight into both the stability of this material and the bonding mechanisms that might apply within the precipitate, the hydrotalcite was washed first with water and then with a strong ion-exchange solution (e.g., 2.5 M  $\text{Na}_2\text{CO}_3$ ). The amount of  $\text{CrO}_4^{2-}$  and  $\text{VO}_4^{3-}$  incorporated into synthetic hydrotalcite was calculated by the difference in the bulk solutions and the residual solutions following in situ precipitation. The 2 mL aliquots of each solution were mixed with 2 mL of 70%  $\text{HNO}_3$  and diluted to 50 mL with demineralized water prior to submission for ICP-MS analysis.

Desorption of transition metal anions was determined using two separate methods of extraction. Hydrotalcite in 0.3 g portions was washed with 40 mL of demineralized water to remove surface adsorbed anions. Other 0.3 g portions were stirred with 10 mL 2.5 M  $\text{Na}_2\text{CO}_3$  for a minimum 30 min followed by addition of 30 mL of demineralized water to remove ion-exchangeable anions. Each solution was then allowed to stand for a minimum of 24 h prior to filtration and drying in air. All filtrates were then mixed with 2 mL of 70%  $\text{HNO}_3$  and diluted to 50 mL with demineralized water prior to submission for ICP-MS analysis. The air-dried samples were analyzed by powder X-ray diffraction.

**2.2. Theoretical.** The model's initial crystal structure was obtained from the previously reported crystal structure of hydrotalcite,  $\text{Mg}_4\text{Al}_2(\text{OH})_{12}\cdot\text{CO}_3\cdot0.3\text{H}_2\text{O}$ . Unit cell of the host structure is trilayer, the space group is  $R\bar{3}\bar{m}$  with triclinic cell and lattice parameters  $a = 3.054 \text{ \AA}$ ,  $c = 23.772 \text{ \AA}$ ,  $\alpha = 90^\circ$ ,  $\beta = 90^\circ$ ,  $\gamma = 120^\circ$ . After removal of  $\text{CO}_3^{2-}$  anions and  $\text{H}_2\text{O}$  molecules, a supercell consisting of  $9a \times 10b \times 2c$  unit cells was built with

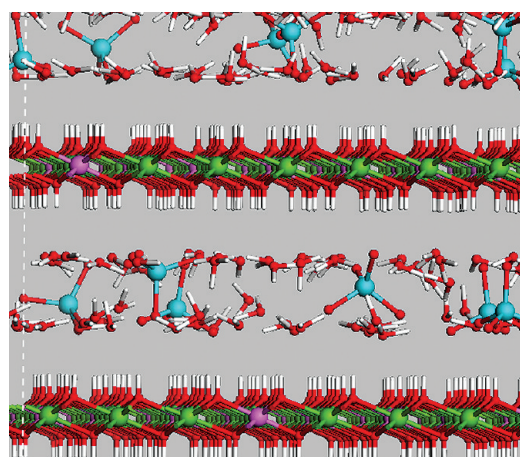


**Figure 1.** Hydrotalcite  $9 \times 10 \times 2$  supercell intercalated with  $\text{VO}_4^{3-}$  anions and water molecules. Green balls represent Mg atoms, pink = Al, gray = hydrogen, and blue = vanadium.

lattice parameters  $9a = 27.486 \text{ \AA}$ ,  $10b = 30.54 \text{ \AA}$ , and  $2c = 15.848 \text{ \AA}$ .

Mg and Al atoms were randomly distributed to obtain the Mg/Al ratio 2:1, each hydroxide layer containing 30 Al and 60 Mg, with a charge on each layer of 30+. Anions totaling to a charge of  $-30$  ( $15 \text{ CO}_3^{2-}$  or  $15\text{CrO}_4^{2-}$  or  $10 \text{ VO}_4^{3-}$  ions) were randomly introduced in between two host layers. Each supercell (Figure 1) constructed had two metal-hydroxide layers and two interlayer galleries, with oxide anion ( $\text{CO}_3^{2-}$ ,  $\text{CrO}_4^{2-}$ , or  $\text{VO}_4^{3-}$ ) charges totaling up to  $-30$  and a variable amount of water molecules,  $30n$ , where  $0 \leq n \leq 15$  (450 water molecules). The typical structural formula of the 2:1 Mg/Al hydrotalcite is  $\text{Mg}_{2n}\text{Al}_n\text{(OH)}_8\text{A}^{x-} \cdot n\text{H}_2\text{O}$ . Similarly, the 4:1 supercell was constructed with 18 Al and 72 Mg atoms resulting with a charge of +18 on each metal-hydroxide layer. Nine  $\text{CO}_3^{2-}$ , 9  $\text{CrO}_4^{2-}$ , or 6  $\text{VO}_4^{3-}$  ions along with 18n water molecules, where  $0 \leq n \leq 25$  (450 water molecules), were introduced between the host layers.

Molecular dynamic simulations were performed using Forceit in Material Studio (MS)<sup>21</sup> 4.4 and 5.5. COMPASS Force Field<sup>22</sup> (which is a general ab initio forcefield) was used for all geometry optimizations and MD simulations. COMPASS is the first high-quality general force field that consolidates parameters for organic and inorganic materials previously found in different force fields. COMPASS force field was assigned to all atoms in the LDH, water, and anions ( $\text{CO}_3^{2-}$ ,  $\text{CrO}_4^{2-}$ , or  $\text{VO}_4^{3-}$ ).

Because layer charge can have a major influence on the anion packing mode in the interlayer, charges for the LDH and water molecules were modified according to the CLAYFF force field of Cygan et al.,<sup>11,22</sup> which is designed to give accurate results for LDH material. Partial charges on all atoms of anions in the gaseous and aqueous phases were calculated by DFT methods. IEF-PCM,<sup>23</sup> the default solvation method implemented in Gaussian 03, was used to calculate the geometry and partial charges of anions in aqueous solution. Geometry optimizations and population analysis of the anions were obtained by using the B3LYP<sup>24,25</sup> method and the LANL2DZ<sup>26</sup> basis set, suitable for transition metals.<sup>27</sup> The LANL2DZ basis set consists of 6-31G-like functions for non-transition-metal atoms and a valence double- $\zeta$  basis set for 3s, 3p, 3d, and 4s electrons and orbitals along with an effective core potential<sup>28</sup> for the metal. These computations were carried out using the Gaussian 03 (G03) program.<sup>29</sup> Partial charges

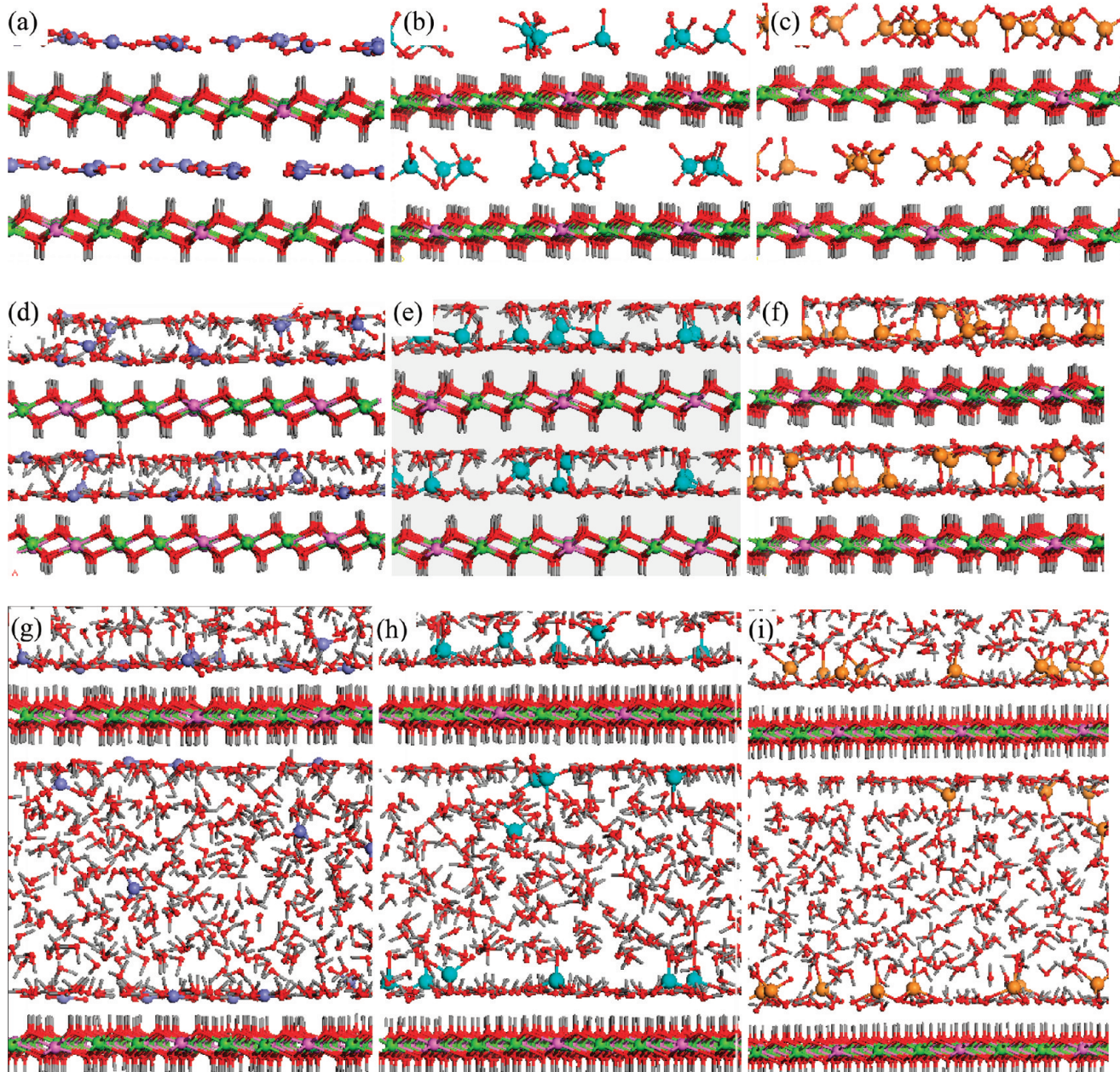


**Figure 2.** Energy minimized structures of 2:1 HT intercalated with carbonates (left column), vanadates (middle column), and chromates (right column) and with increasing number of water molecules. First row,  $n = 0$ , second row,  $n = 3$  (90 water molecules in each interlayer), and third row,  $n = 15$  (450 water molecules in each interlayer).

were obtained from Natural Population Analysis (NPA)<sup>30</sup> using the NBO program in G03.

Prior to MD simulations geometry optimizations of the hydrotalcite intercalated with anions and water molecules were carried out. The electrostatic and van der Waals energies were calculated by the Ewald summation method and minimizations carried out by Quasi-Newton procedure. Periodic boundary conditions were applied in three dimensions so that the simulation cell is effectively repeated infinitely in each direction. Initially the host layers in the supercell were held as rigid units allowing the lattice parameter  $c$  (gallery height) to vary. The structures of the anions were also held rigid using the “keep motion groups rigid” function available in geometry optimization in Forcite. This enabled the mutual positions of the host layers and positions

and orientations of the guest layers (anions and water molecules) to vary and optimize to a minimum with respect to each other. These optimized structures were then used as the starting configurations for the MD simulations, performed in the NVT-ensemble (constant-volume/constant-temperature) where atoms in both the host and the guest layers were released. Because all atoms in each system were completely free to move during these simulations, using the constant-volume modeling approach with a fixed cell shape does not introduce significant limitations to the resulting interfacial structure, dynamics, and energetics of water.

MD simulations were performed in NVT-ensemble at 300 K and a time step of 1.0 fs was used for all simulations. Analysis of the simulations revealed that equilibrium values for the thermodynamic

parameters were generally reached within the first 20 ps using an Andersen thermostat. An initial MD simulation of 30 ps was carried out using Andersen thermostat followed by 200 ps simulations with Nosé thermostat for different hydration states,  $n$ , of the system.

Hydration energies have been found to be a simple and effective measure of the affinity of water for the interlayer.<sup>14,16,17</sup> Hydration energy of a system is defined as

$$\Delta U_H(N_w) = \frac{\langle U_H(N_w) \rangle - \langle U(0) \rangle}{N_w} \quad (1)$$

where  $N_w$  is the number of water molecules and  $U(N_w)$  and  $U(0)$  are the total potential energies of the system with  $N_w$  and zero water molecules, respectively.

To study the interactions of water molecules and anions in bulk water (i.e., aqueous suspensions), 450 water molecules were placed in each interlayer space and longer NVE-ensemble MD simulations of 400 ps duration, including an initial 50 ps time for equilibration, were carried out to calculate the mean square displacement (MSD), self-diffusion coefficient, and concentration profiles.

The REFLEX module in Material Studio (MS) 5.5 was used to calculate the powder X-ray diffraction (PXRD) patterns of the optimized structures of LDH. To match the model with the experimental setup, the radiation wavelength was set to 1.540598 Å and the diffractometer range  $2\theta$  was set from 4 to 40°, with a step size of 0.05°.

### 3. RESULTS

The systems studied here are designed to reflect compositions of the two hydrotalcites commonly found in the seawater

**Table 1. Partial Charges and Bond Lengths of Anions with Water as the Solvent Calculated at B3LYP/LANL2DZ, with the IEF-PCM Solvation Model**

anion	atom	partial charge ( $e$ )	bond length		symmetry
			(Å)	(X–O)*	
$\text{CO}_3^{2-}$	C	0.966 (0.969)	1.333 (1.344)		$C_{2v}$
	O	-0.989 (-0.990)			
$\text{VO}_4^{3-}$	V	0.959 (0.842)	1.727 (1.753)		$T_D$
	O	-0.990 (-0.961)			
$\text{CrO}_4^{2-}$	Cr	0.813 (0.826)	1.657 (1.667)		$T_D$
	O	-0.703 (-0.706)			

\*X = C, V, or Cr, and the values in parentheses are with no solvent.

neutralization system and on the seafloor, that is,  $[\text{Mg}_{0.67}\text{Al}_{0.33}(\text{OH})_2][\text{A}^{2-}]_{0.16} \cdot 2\text{H}_2\text{O}$  (2:1 hydrotalcite) and  $[\text{Mg}_{0.80}\text{Al}_{0.20}(\text{OH})_2][\text{A}^{2-}]_{0.10} \cdot 2\text{H}_2\text{O}$  (4:1 hydrotalcite). The range of intercalates has been limited to include the common Bayer process anions  $\text{CO}_3^{2-}$  and two transition metal anions of interest,  $\text{VO}_4^{3-}$  and  $\text{CrO}_4^{2-}$ .

**3.1. Modeling Results.** **3.1.1. Anion Partial Charges.** Structures of the anions optimized at B3LYP/LANL2DZ are shown embedded in Figure 2. The calculated partial charges and bond lengths of anions with and without water as the solvent are given in Table 1.

The calculated Cr–O bond length of the tetrahedral chromate ion is close to the experimental bond length of 1.66 Å in the chromate anion in solution as reported by Hoffman et al.<sup>31</sup> The V–O bond length of 1.69–1.75 Å is reported by Dolgos et al.<sup>32</sup> for different vanadate salts.

**3.1.2. HT Swelling Energetics.** Optimized structures, where intercalated anions as well as water molecules were allowed to relax, but with fixed LDH layers, are shown in Figure 2.

In carbonate-HT, the trigonal planar  $\text{CO}_3^{2-}$  ions lie horizontally in the interlayer in the absence of water molecules. As the number of water molecules is increased, they orient themselves perpendicular to the LDH layer. In the vanadate and chromate-HT, the tetrahedral  $\text{VO}_4^{3-}$  and  $\text{CrO}_4^{2-}$  ions have two orientations in the absence of water molecules. One orientation has three oxygen atoms forming hydrogen bonds with one LDH layer and the fourth oxygen with the other LDH layer. The second orientation has two oxygen atoms each hydrogen bonding with OH groups of LDH layer. As the water content in the interlayer is increased, the  $d$ -spacing increases very slowly as the water molecules fill the empty space between the anions and form hydrogen bonds with the oxygen atoms of the anion and the hydroxide groups in the LDH (Figure 2d–f).

As shown in Figure 3, once the water content is above  $n = 2$  (in 2:1 HT), a new water layer is formed and the  $d$ -spacing takes the pop-and-fill pattern (Figure 3a) with increasing water content. In 4:1 HT (Figure 3b), a new water layer is formed after  $n = 4$ , because there are a lesser number of anions in the interlayer and, hence, more water molecules can be filled into the first water layers. Carbonate-HT's show a slightly different trend in the beginning as they switch from lying horizontal, that is, parallel, to the metal hydroxide layer until  $n = 2$  in 2:1 and  $n = 4$  in 4:1 HT and shifting to a perpendicular position afterward, but continuing with the pop-and-fill pattern. The water molecules form highly ordered layers with oxygen atoms orienting toward the LDH layer and the hydrogen atoms orienting away from the hydroxide layers.

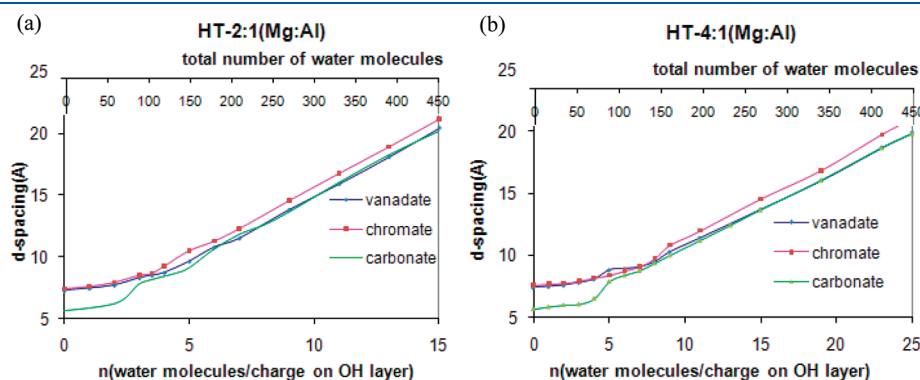


**Figure 3.** Variation of  $d$ -spacing (interlayer distance) as a function of the number of water molecules ( $n$ ) per charge on the metal hydroxide layer.

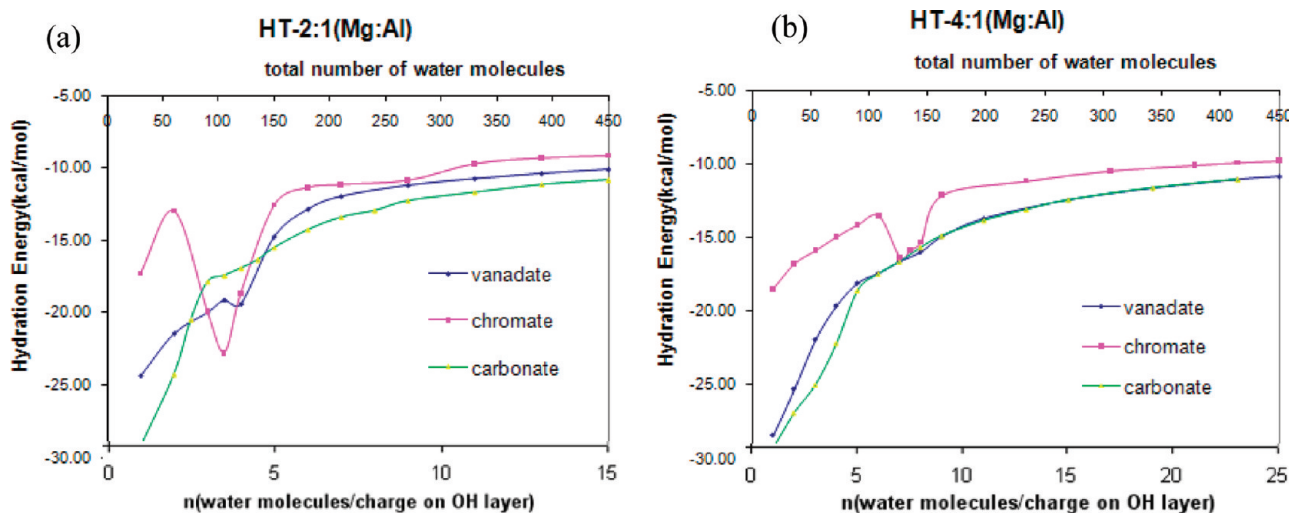


**Figure 4.** Variation of hydration energy ( $\Delta U_H(N_w)$ ) as a function of the number of water molecules ( $n$ ) per charge on the metal hydroxide layer and total number of water molecules in each interlayer.

This in turn induces further ordered water (OW) layers away from the LDH layer. However, as the distance of the water layers from the LDH layer increases, disorder increases. The average distance between the H atoms in the LDH layer and the oxygen atoms of the first OW layer in 2:1 water is around 1.80–1.90 Å, while that in 4:1 HT is 2.12–2.13 Å. This is mainly due to the weaker charge on the LDH layer in 4:1 HTs.

Hydration energies (HE) computed are plotted against the number of water molecules ( $n$ ) per charge on the LDH layer in Figure 4. Similar to most of the previous studies on organic anions,<sup>17</sup> hydration energy shows the largest negative values at low water content and increases as the water content increases. The hydration energy (eq 1) has several components, including the potential energy of interlayer water, the effects on the potential energy of changing interactions of the hydroxide layers with themselves and the anions, and the anions with themselves. Hydration energy is therefore the sum of energy required to expand an equilibrium structure to create additional interlayer space for more water molecules and the energy gained due to the presence of additional water molecules, rearrangement of interlayer species, reformation of the hydrogen bonding network, and equilibration of the system in a new hydration state. A minimum if observed in the hydration energy on addition of water molecules indicates a preferred hydration state of the system. This can be interpreted as arising from the well-developed hydrogen-bonding network as more water molecules are added.

For 2:1 systems,  $\Delta U_H(N_w)$  values increase rapidly with increasing water content. Chromate-HT exhibit a decrease in hydration energy after  $n = 2$ , with a minimum at  $n = 3.5$ . The vanadate-HT, has a minimum at  $n = 4$ , while the carbonate-HT do not exhibit a minimum, but only a plateau between  $n = 3$  and 4. Comparing this with results in Figure 3, it is seen that the minima coincide with the plateauing of the  $d$ -spacing or filling up of the first OW layer. After  $n = 5$ , as the water content further increases, for all three HTs, the  $\Delta U_H(N_w)$  values increase at a very slow rate and plateau almost parallel to each other. The hydration energies of all three HTs approach the bulk water potential energy ( $\sim -10$  kcal/mol<sup>14,17</sup>) value. Carbonate- and vanadate-HT have lower  $\Delta U_H(N_w)$  values compared to chromate-HT. Carbonate-HT has the lowest value, which indicates

its stronger affinity to water at all phases of water content in 2:1 HT only.

In the 4:1 systems, only the chromate-HT exhibits a minimum in the hydration energy values at  $n = 7$ , while vanadate- and carbonate-HT show a slow increase in that region. It is important to note here that the total number of water molecules of the 4:1 HT at  $n = 7$  is similar to  $n = 4$  of 2:1 HTs, that is,  $\sim 120$  water molecules per interlayer. Like the 2:1 HT systems, the hydration energies of all three HTs approach the bulk water potential energy value. Chromate-HT has higher hydration energy than vanadate and carbonate-HT, and it is also interesting to note that the HE of the vanadate-HT and carbonate-HTs are very similar in the 4:1 systems.

**3.1.3. Anions in Interlayer.** To model the relative positions of the anions and water molecules in water-rich environments, such as high humidity conditions or in aqueous suspensions, longer simulations were carried out with 450 water molecules in each interlayer. The atomic density profiles along the  $z$ -direction, obtained from 500 ps of fully relaxed (NVE ensemble) MD simulations of the LDH with 450 water molecules in each interlayer, is shown in Figure 5.

Water molecules form two distinct ordered water (OW) layers in all HTs. Results show that most of the anions (represented by blue line) prefer to position themselves close to the first OW layer in both the 2:1 HT and 4:1 HTs. The chromate and the vanadate anions are found to be positioned between the first and the second OW layers. One or three oxygen atoms are in plane with the first OW layer and form hydrogen bonds with both the water molecules and the LDH layer, while the remaining oxygen atoms (3 or 1) are situated in the second OW layer. A majority of the anions prefer the orientation where the three oxygen atoms are in the first OW layer. As a result, the metal atom of the anion is located just above the first OW layer as seen both in Figure 2 and the atomic density profiles in Figure 5.

The carbon and the oxygen atoms in the planar carbonate ions orient themselves parallel to the LDH layer and along the first OW layer in the water-rich HTs, but in the preferred or optimal water content situations (Figure 2d) they are found to orient predominantly perpendicular to the LDH layer. The simulations indicate that, in general, the chromate ions are found only in the first OW layer. In comparison, the majority of the vanadate and

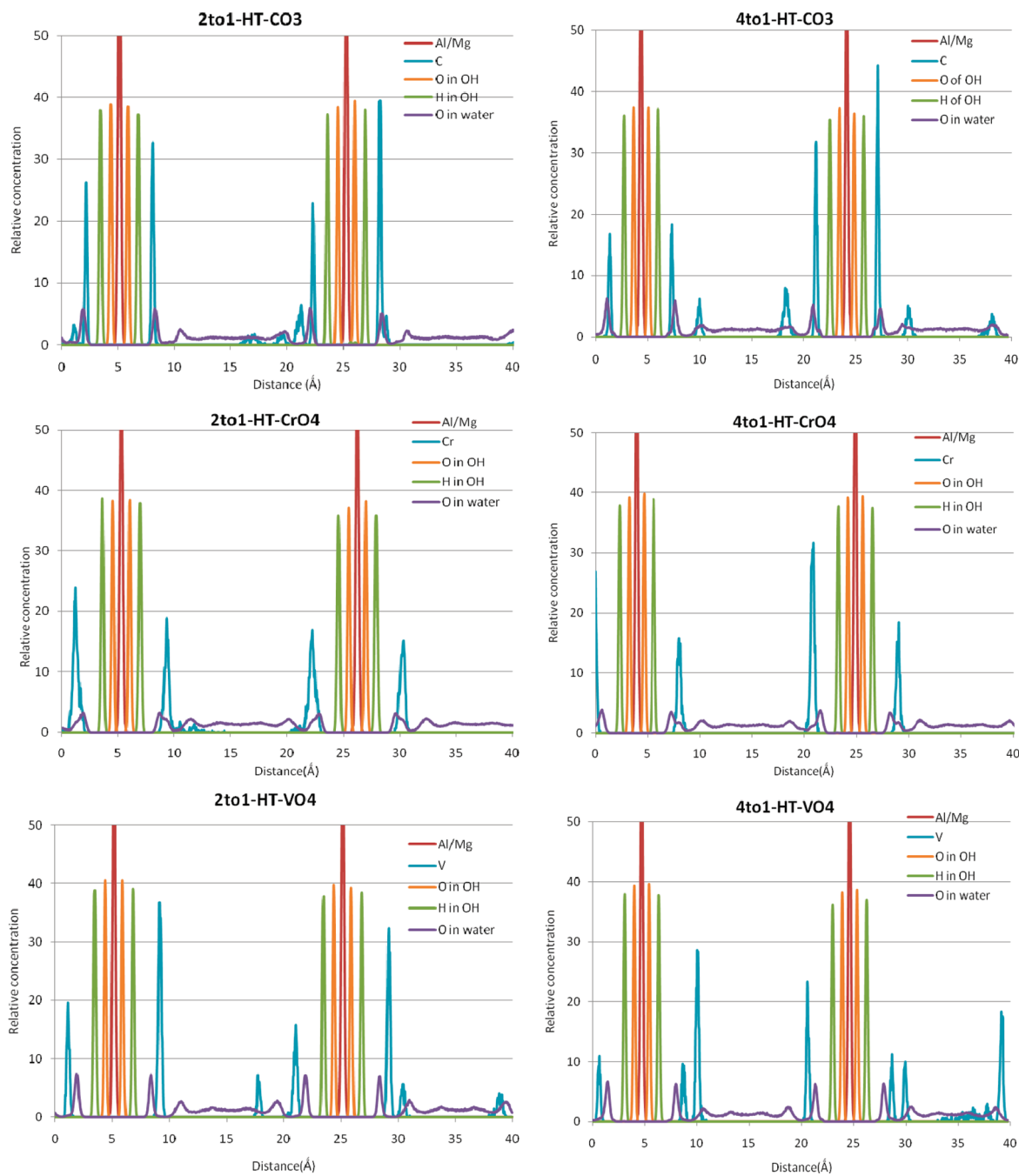


**Figure 5.** Atomic density profiles along the  $z$ -direction of the supercell obtained from 500 ps of fully relaxed MD simulations of the LDH with 450 water molecules in each interlayer.

carbonate ions are also found in the first OW layer, but some are found in the second OW layer.

To study the relative mobility of the anions in both the 2:1 and 4:1 HTs, self-diffusion coefficients ( $D$ ) were calculated from the mean square displacements (MSD) of anions and the water molecules in different OW layers; and in the middle of the interlayer space, using fully relaxed NVE models, with MD simulation of 300 ps, at 300 K. Calculated  $D$  from the simulations are presented in Table 2 and plotted in Figure 6 for comparison. MSDs are also calculated for the optimal or preferred water states for all HTs, such as  $n = 3.5$  and 4 for chromate and vanadate 2:1 HTs, respectively.

The results indicate that the anions in the 2:1 HTs have lower self-diffusion coefficients ( $D$ ) in comparison to 4:1 systems. In both the 2:1 and the 4:1 HT, the  $D$  value increases as the distance the anion is from the LDH layer increases. The diffusion of water molecules in various ordered and disordered layers follow the same trend. As the distance of the water molecules from the hydroxide layer increases,  $D$  increases.  $D$  values of water in the first OW layer for the 2:1 HTs change slower than the 4:1 HTs (similar to the anions), but they increase rapidly and are higher than the  $D$  values of 4:1 systems in layer 2 and midgallery positions. The bulk water self-diffusion coefficient calculated under the same simulation conditions (as stated in the theoretical methods

section (at 300 K)) is determined to be  $3.2 \times 10^{-5} \text{ cm}^2/\text{s}$ . This value of  $D$  is slightly higher than the experimental self-diffusion coefficient of water between 298 and 305 K, reported as  $2.3 \times 10^{-5} \text{ cm}^2/\text{s}$  to  $2.9 \times 10^{-5} \text{ cm}^2/\text{s}$ .<sup>33,34</sup> A  $D$  value of  $3.2 \times 10^{-5} \text{ cm}^2/\text{s}$  using COMPASS FF has also been observed elsewhere.<sup>35</sup> Simulations were also run for a salt solution

**Table 2.** Self Diffusion Coefficient ( $D$ ) of Anions and Water Molecules in Bulk Water (450 Water Molecules in Each Interlayer) Calculated from Fully Relaxed MD Simulation for 300 ps, at 300 K

self-diffusion coefficient ( $\text{cm}^2/\text{s}$ )			
	$\text{CO}_3^{2-}$	$\text{CrO}_4^{2-}$	$\text{VO}_4^{3-}$
2:1 HT			
ions in layer 1	$2.02 \times 10^{-7}$	$7.84 \times 10^{-7}$	$8.08 \times 10^{-8}$
ions in midgallery	$1.11 \times 10^{-6}$		$7.19 \times 10^{-7}$
water in layer 1	$7.34 \times 10^{-6}$	$8.90 \times 10^{-6}$	$4.90 \times 10^{-6}$
water in layer 2	$1.72 \times 10^{-5}$	$2.17 \times 10^{-5}$	$1.64 \times 10^{-5}$
water in midgallery	$1.89 \times 10^{-5}$	$2.34 \times 10^{-5}$	$2.00 \times 10^{-5}$
4:1 HT			
ions in layer 1	$3.82 \times 10^{-7}$	$2.03 \times 10^{-6}$	$6.34 \times 10^{-7}$
ions in layer 2	$1.05 \times 10^{-6}$		
ions in midgallery	$2.85 \times 10^{-6}$		$4.50 \times 10^{-6}$
water in layer 1	$1.36 \times 10^{-5}$	$1.70 \times 10^{-5}$	$1.07 \times 10^{-5}$
water in layer 2	$1.48 \times 10^{-5}$	$2.07 \times 10^{-5}$	$1.67 \times 10^{-5}$
water in midgallery	$1.74 \times 10^{-5}$	$2.24 \times 10^{-5}$	$1.76 \times 10^{-5}$

( $\text{MgCl}_2$ ) of the same ionic strength as the HT systems studied here. The calculated  $D$  for the salt solution was found to be  $2.34 \times 10^{-5} \text{ cm}^2/\text{s}$ . As shown in Table 2,  $D$  of water in the middle of the gallery in chromate-2:1 HT has the same value and is the highest compared to all systems studied here.

$D$  values were calculated from MSDs for the optimal or preferred water states (see Figure 4) for all HTs. They are shown in Table 3, while Figure 7 shows the self-diffusion of anions in both 2:1 and 4:1 systems.

**3.2. Experimental Results.** Powder X-ray diffraction patterns for HT with different interlamellar anions and Mg/Al ratios

### *D of ions*

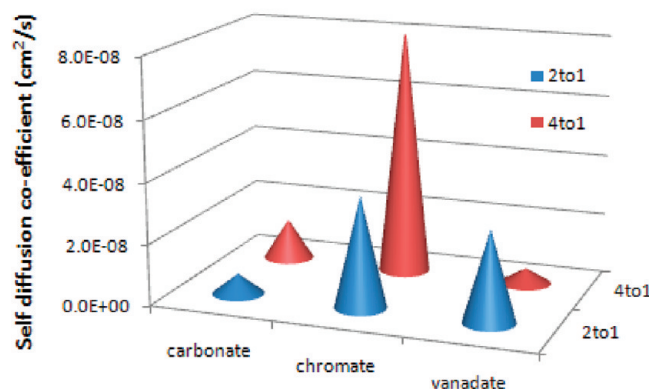


**Figure 7.** Self-diffusion coefficient ( $D$ ) of anions in preferred water state HTs.

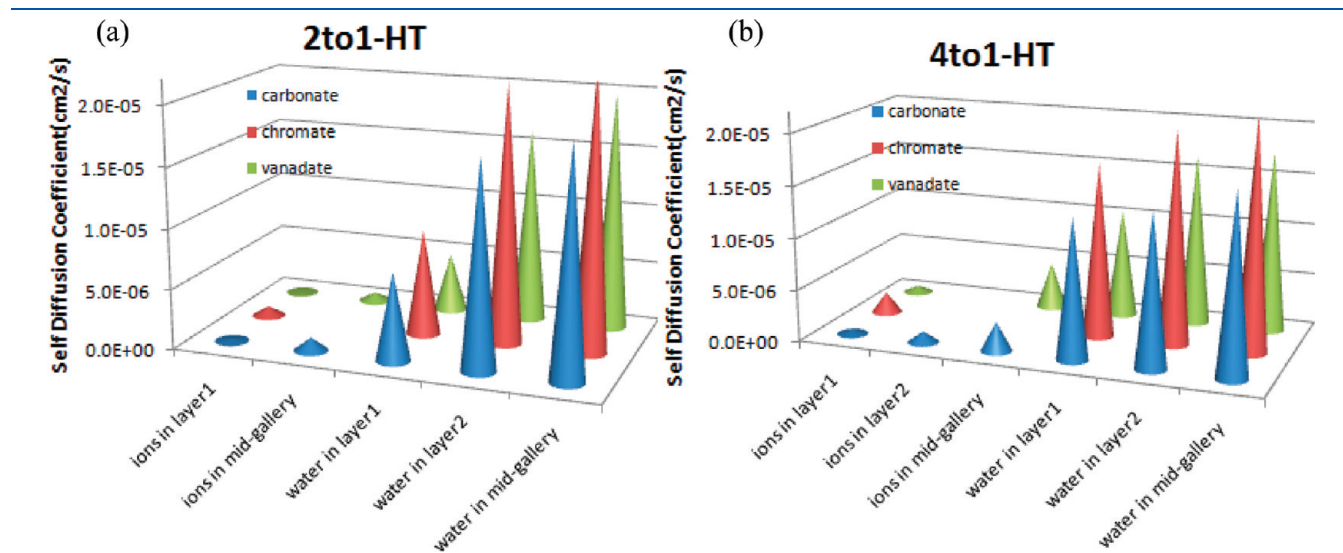


**Figure 6.** Comparative self-diffusion coefficient ( $D$ ) in  $\text{cm}^2/\text{s}$  of anions and water molecules calculated from fully relaxed MD simulation for 500 ps, at 300 K for 2:1 and 4:1 HTs.

**Table 3.** Self-Diffusion Coefficient ( $D$ ) of Anions and Water Molecules in Preferred Water State HTs Calculated from Fully Relaxed MD Simulation for 300 ps, at 300 K

self-diffusion coefficient ( $\text{cm}^2/\text{s}$ )					
	$\text{CO}_3^{2-}$	water	$\text{CrO}_4^{2-}$	water	$\text{VO}_4^{3-}$
2:1 HT	$6.67 \times 10^{-9}$	$1.50 \times 10^{-7}$	$3.67 \times 10^{-8}$	$1.92 \times 10^{-7}$	$3.00 \times 10^{-8}$
4:1 HT	$1.33 \times 10^{-8}$	$1.46 \times 10^{-6}$	$8.33 \times 10^{-8}$	$1.31 \times 10^{-6}$	$5.00 \times 10^{-9}$

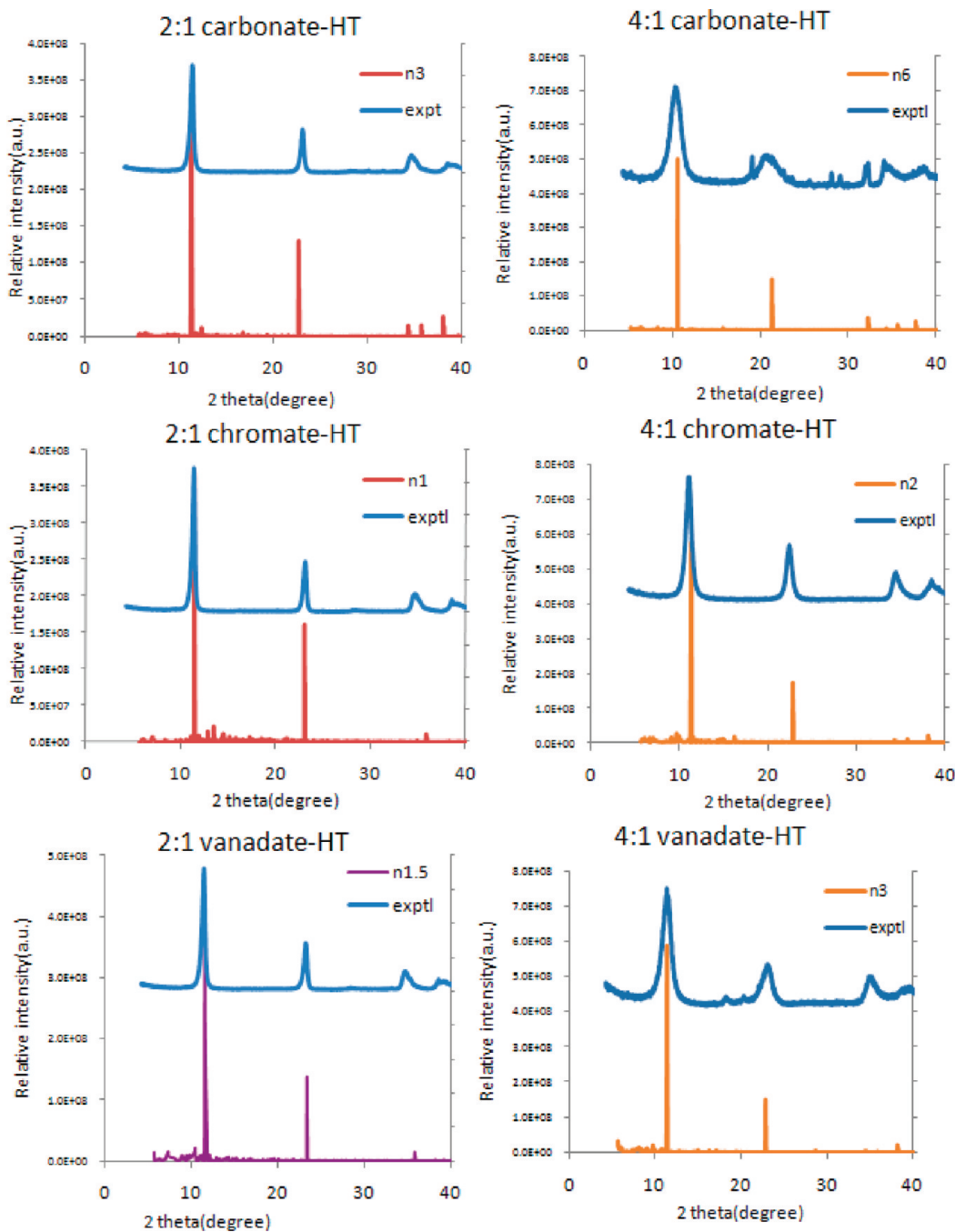


Figure 8. Experimental and calculated PXRD patterns of 2:1 and 4:1 hydrotalcites.

(as indicated in section 2) were obtained using Co K $\alpha$  radiation on a Philips PW3710 diffractometer using a  $2\theta$  step size of 0.020 and a PW1752 diffracted beam monochromator with receiving slit height of 0.2 mm. Where diffraction patterns were poor, greater sensitivity was obtained by reducing  $2\theta$  step size and increasing analysis time. The calculated powder X-ray diffraction (XRD) pattern of the optimized LHD structures and the experimental diffraction pattern of hydrotalcites intercalated with different anions and Mg/Al ratio are shown in Figure 8. In Table 4, the  $d$ -spacing of HT obtained experimentally is compared against the water content in the corresponding calculated LHD structures. This provides a measure of the

variability of water content for different anion and Mg/Al ratios in the air-dried samples of HT.

Data presented in Table 5 shows variability in the ability of hydrotalcite to recover and retain transition metal anions across anion type and Mg/Al ratio. The initial step of washing the hydrotalcite with water removes any surface and loosely bound anions. The next step of washing with a carbonate solution gives an indication of the ability of the carbonate ions to remove the intercalated oxymetal anions (i.e., vanadate and chromate). Carbonate was used as an ion-exchange medium because it is believed to be the most preferred intercalating anion known and is capable of exchanging  $\text{CrO}_4^{2-}$  and  $\text{VO}_4^{3-}$  contained within

the hydrotalcite matrix. The high residual amounts of  $\text{VO}_4^{3-}$  and  $\text{CrO}_4^{2-}$  indicate that complete ion-exchange does not occur.

The degree of variability between residual amounts of  $\text{CrO}_4^{2-}$  and  $\text{VO}_4^{3-}$  suggest that anion-exchange capacity is dependent not only upon electrostatic charge interaction but also on Mg/Al ratio. It is seen that while there is a higher retention of chromate ions in 2:1 HT (83.3%) compared to 4:1 HT (57.7%), vanadates ions show an opposite trend, that is, 92% of vanadates ions are retained in 4:1 HT, while only 60.1% retained in 2:1 HT.

#### 4. INTERPRETATION OF EXPERIMENTAL AND MODELING RESULTS

Due to the LDH layer charges, the electrostatic forces of attraction would be stronger in 2:1 HT compared to 4:1 HT. This is also reflected in the modeling results where the anions are held closer to the LDH layers in the first OW layer compared to 4:1 HTs. The calculated distance of the first OW layer from the H atoms in the LDH layer is 1.8–1.9 Å for the 2:1 HTs compared to 2.12–2.13 Å in the 4:1 HTs. The variable water content (refer Table 4) in the air-dried samples of different HTs is well justified, as 2:1 HTs contain less water compared to 4:1 HTs as the 4:1 HTs have fewer anions compared to the 2:1 HTs. Vanadate-HTs have slightly more water content compared to chromate-HT owing to the charge on vanadate being –3 and, hence, there are fewer ions in the interlayer. Even though the carbonate ions have the same charge as the chromate ions, the higher number of water in the carbonate-HTs can also be well justified, as there are only three oxygen atoms in each carbonate ion and more water molecules are required to compensate for the lower number of oxygen atoms in the carbonate ions.

The preferred or optimal hydration states indicated by the minima in the hydration energy values along with the hydration states where the hydration energy plateaus (for systems with no minima) is tabulated in Table 6. The water molecules in these states are found to form two water layers (as shown in Figure 2d–f) forming a network of hydrogen bonds with the H atoms on the metal hydroxide layer. The anions are found to

position themselves in between these two water layers with the oxygen atoms embedded in the water layers. The variability in the amount of water molecules per water layer is compensated by the number of oxygen atoms from the anions. The total number of oxygen atoms in each water layer is found to be around 82, in both 2:1 and 4:1 chromate- and vanadate-HTs. The lower number of oxygen atoms in the 2:1 carbonate-HT can be attributed to the fact that the planar carbonate ions predominantly position themselves horizontally in the water layer. This brings the total number of atoms, oxygen plus carbon, to 82 per layer. The higher number of water molecules per layer in the 4:1 carbonate-HT indicates that the carbonate ions are positioned perpendicular to the water layer with only one oxygen atom embedded in the water layer. This also facilitates closer packing of water molecules in the water layers and, hence, a higher gallery height or *d*-spacing observed experimentally for 4:1 carbonate-HT.

The relative mobility of the anions and the water molecules in the interlayer of hydrotalcites in water rich environments, such as aqueous suspensions, can be studied by comparing the self-diffusion coefficients (*D*). The vanadate ions have a smaller *D* value (Figure 6) compared to chromate ions in both 2:1 and 4:1 HTs. Water molecules in the first OW of vanadate-HT are also less mobile compared to waters in the first OW layer of chromate-HT. This is because the oxygen atoms in the vanadate ions have larger partial negative charge of –0.961e (Table 1) compared to the oxygen atoms in the chromate ions (–0.706e). The vanadate ions in the first layer are stabilized by forming stronger hydrogen bonds with the metal hydroxide layer. Water in the middle of the gallery in chromate-HT is free of any

**Table 6. Comparison of Water Content (*n*) in Preferred Hydration States along with Total Number of Water Molecules and Anions in Each Interlayer**

anions	<i>n</i>	H <sub>2</sub> O molecules	O atoms in anions	total O atoms (H <sub>2</sub> O + anion)
2:1 HT				
$\text{CrO}_4^{2-}$	3.5	105	15	60
$\text{VO}_4^{3-}$	4	120	10	40
$\text{CO}_3^{2-}$	3.5 <sup>a</sup>	105	15	45
4:1 HT				
$\text{CrO}_4^{2-}$	7	126	9	36
$\text{VO}_4^{3-}$	8 <sup>a</sup>	144	6	24
$\text{CO}_3^{2-}$	9 <sup>a</sup>	162	9	27

<sup>a</sup> Hydration states corresponding to a plateau or decrease in the change of hydration energy.

**Table 4. Experimental *d*-Spacing and the Corresponding Water Content from Calculated Patterns**

anion	2:1 HT		4:1 HT	
	experimental <i>d</i> -spacing	<i>n</i> (water content)	experimental <i>d</i> -spacing	<i>n</i> (water content)
$\text{CrO}_4^{2-}$	7.71 Å	1	7.92 Å	2
$\text{VO}_4^{3-}$	7.64 Å	1.5	7.76 Å	3
$\text{CO}_3^{2-}$	7.67 Å	3	8.71 Å	6

**Table 5. In Situ Anion Recovered During Precipitation of Hydrotalcite (HT)<sup>a</sup>**

anion	adsorbed (water washed)	ion-exchanged ( $\text{CO}_3^{2-}$ washed)	residual (intercalated)
$\text{VO}_4^{3-}$	9.7%	$[\text{Mg}_{0.67}\text{Al}_{0.33}(\text{OH})_2](\text{A}^{n-})_{0.16} \cdot x\text{H}_2\text{O}$ (pH > 12) 2:1 HT	60.1%
$\text{CrO}_4^{2-}$	3.7%	30.2%	83.3%
		12.8%	
		$[\text{Mg}_{0.80}\text{Al}_{0.20}(\text{OH})_2](\text{A}^{n-})_{0.10} \cdot x\text{H}_2\text{O}$ (pH < 10) 4:1 HT	
$\text{VO}_4^{3-}$	0.5%	7.4%	92.1%
$\text{CrO}_4^{2-}$	14.3%	28.0%	57.7%

<sup>a</sup> The values expressed represent the amount of  $\text{CrO}_4^{2-}$  and  $\text{VO}_4^{3-}$  recovered from the bulk solutions.

chromate ions (Figure 5) and forms a bulk-water-like hydrogen bonding network with a  $D$  value reaching  $2.34 \times 10^{-5} \text{ cm}^2/\text{s}$  in 2:1 HT (Table 2). This is similar to the  $D$  value obtained for bulk water with similar ionic strength as shown in section 3.1. A few vanadate and carbonate ions are found to migrate to the middle of the gallery forming hydrogen bonds with the water molecules indicated by a lower  $D$  value for the water in vanadate- and carbonate-HTs.

Hydration energy calculations performed with different water contents show a well-defined minimum for chromate in both 2:1 and 4:1 HTs. Analysis of the  $D$  values obtained for the interlayer species in these preferred hydration states (Figure 7) shows a lower  $D$  value for chromate ions in 2:1 compared to 4:1 HT, supporting the increased retention of chromate ions observed experimentally in the 2:1 system (Table 5). Also, examination of the minimum in the hydration energy value (Figure 4a) for chromate in 2:1 system is lower than the corresponding vanadate and carbonate system in the same water regime, indicating that there is a greater degree of stabilization of the chromate-HT in the preferred hydration state in 2:1.

Taking a closer look at the hydration energy variation for 4:1 system (Figure 4b) we can see that the minimum in the hydration energy of chromate-HT lies above the corresponding hydration energy for vanadate-HT. This could be due to the hydrogen bonds donated to the vanadate ions by the water molecules are not energetically preferable, and the vanadate ions are stabilized by hydrogen bonds donated from the metal hydroxide layer. Comparison of the  $D$  values for 2:1 and 4:1 (Figure 7) shows that the vanadate ions in the 4:1 vanadate-HT have the lowest  $D$  value, indicating low mobility of the vanadate ions. This supports the higher retention of vanadate ions in the 4:1 system observed experimentally.

## 5. CONCLUSION

The arrangement and mobility of interlayer species in LDH structures of different Mg/Al ratios and different oxymetal anions can be studied using COMPASS forcefield in combination with CLAYFF charges on metal hydroxide layer and partial charges on anions obtained from DFT methods. Hydration energy values obtained from MD simulations of the hydrotalcite for different hydration states or water content provide a good indication of the stability of the HT.

A well-defined minima in the hydration energy of chromate-HT suggests that it has an energetically well-defined structural state at specific water content and that chromate-HT is stabilized by the formation of hydrogen bonds between the metal hydroxide and the chromate ions with the water molecules. The absence of the well-defined minima in vanadate-HT with different water content indicates that it would absorb water continuously in aqueous suspensions leading to delamination. However, the low mobility of the vanadate ions intercalated suggests that the vanadate-HT are stabilized by hydrogen bonds donated from the metal hydroxide layer. Hence vanadate ions are strongly held by electrostatic attraction and hydrogen bonding with the metal hydroxide layer and vanadates would stay bound once intercalated. The higher retention of vanadate ions in 4:1 HT observed experimentally could also be due to the substitution of vanadium into the metal hydroxide layer which has not been investigated in this study.

## ■ AUTHOR INFORMATION

### Corresponding Author

\*Tel.: +61 439680172. E-mail: vinuthaa.murthy@cdu.edu.au.

## ■ REFERENCES

- (1) Smith, H. D.; Parkinson, G. M.; Hart, R. D. *J. Cryst. Growth* **2005**, 275, e1665.
- (2) Menzies, N. W.; Fulton, I. M.; Morrell, W. J. *J. Environ. Qual.* **2004**, 33, 1877.
- (3) Koumanova, B.; Drame, M.; Popangelova, M. *Resour., Conserv. Recycl.* **1997**, 19, 11.
- (4) Palmer, S. J.; Frost, R. L. *Ind. Eng. Chem. Res.* **2010**, 49, 8969.
- (5) Palmer, S. J.; Frost, R. L.; Nguyen, T. *Coord. Chem. Rev.* **2009**, 253, 250.
- (6) Prasanna, S. V.; Vishnu Kamath, P. *Solid State Sci.* **2008**, 10, 260.
- (7) Aicken, A. M.; Iain, S. B.; Peter, V. C.; William, J. *Adv. Mater.* **1997**, 9, 496.
- (8) Fogg, A. M.; Rohl, A. L.; Parkinson, G. M.; O'Hare, D. *Chem. Mater.* **1999**, 11, 1194.
- (9) Rives, V.; Angeles Ulibarri, M. *Coord. Chem. Rev.* **1999**, 181, 61.
- (10) Wang, J.; Kalinichev, A. G.; Amonette, J. E.; Kirkpatrick, R. J. *Am. Mineral.* **2003**, 88, 398.
- (11) Cygan, R. T.; Liang, J.-J.; Kalinichev, A. G. *J. Phys. Chem. B* **2004**, 108, 1255.
- (12) Zhang, H.; Xu, Z. P.; Lu, G. Q.; Smith, S. C. *J. Phys. Chem. C* **2008**, 113, 559.
- (13) Kovář, P.; Pospíšil, M.; Nocchetti, M.; Čapková, P.; Melánová, K. *J. Mol. Model.* **2007**, 13, 937.
- (14) Smith, D. E. *Langmuir* **1998**, 14, 5959.
- (15) Padma Kumar, P.; Kalinichev, A. G.; Kirkpatrick, R. J. *J. Phys. Chem. B* **2006**, 110, 3841.
- (16) Wang, J.; Kalinichev, A. G.; Kirkpatrick, R. J.; Cygan, R. T. *J. Phys. Chem. B* **2005**, 109, 15893.
- (17) Kumar, P. P.; Kalinichev, A. G.; Kirkpatrick, R. J. *J. Phys. Chem. C* **2007**, 111, 13517.
- (18) Newman, S. P.; Di Cristina, T.; Coveney, P. V.; Jones, W. *Langmuir* **2002**, 18, 2933.
- (19) Hou, X.; Bish, D. L.; Wang, S.-L.; Johnston, C. T.; Kirkpatrick, R. J. *Am. Mineral.* **2003**, 88, 167.
- (20) Kalinichev, A. G.; Padma Kumar, P.; James Kirkpatrick, R. *Philos. Mag.* **2010**, 90, 2475.
- (21) Accelrys Software, Inc. *M. Material Studio (MS)*.
- (22) Cygan, R. T.; Greathouse, J. A.; Heinz, H.; Kalinichev, A. G. *J. Mater. Chem.* **2009**, 19, 2470.
- (23) Tomasi, J.; Mennucci, B.; Cancès, E. *J. Mol. Struct.: THEOCHEM* **1999**, 464, 211.
- (24) Becke, A. D. *J. Chem. Phys.* **1988**, 88, 1053.
- (25) Becke, A. D. *J. Chem. Phys.* **1993**, 98, 5648.
- (26) Wadt, W. R.; Hay, P. J. *J. Chem. Phys.* **1985**, 82, 284.
- (27) Hedegård, E. D.; Bendix, J.; Sauer, S. P. *A. J. Mol. Struct.: THEOCHEM* **2009**, 913, 1.
- (28) Hay, P. J.; Wadt, W. R. *J. Chem. Phys.* **1985**, 82, 299.
- (29) Frisch, M. J.; Trucks, G. W.; Schlegel, H. B.; Scuseria, G. E.; Robb, M. A.; Cheeseman, J. R.; Montgomery, Jr., J. A.; Vreven, T.; Kudin, K. N.; Burant, J. C.; Millam, J. M.; Iyengar, S. S.; Tomasi, J.; Barone, V.; Mennucci, B.; Cossi, M.; Scalmani, G.; Rega, N.; Petersson, G. A.; Nakatsuji, H.; Hada, M.; Ehara, M.; Toyota, K.; Fukuda, R.; Hasegawa, J.; Ishida, M.; Nakajima, T.; Honda, Y.; Kitao, O.; Nakai, H.; Klene, M.; Li, X.; Knox, J. E.; Hratchian, H. P.; Cross, J. B.; Adamo, C.; Jaramillo, J.; Gomperts, R.; Stratmann, R. E.; Yazev, O.; Austin, A. J.; Cammi, R.; Pomelli, C.; Ochterski, J. W.; Ayala, P. Y.; Morokuma, K.; Voth, G. A.; Salvador, P.; Dannenberg, J. J.; Zakrzewski, V. G.; Dapprich, S.; Daniels, A. D.; Strain, M. C.; Farkas, O.; Malick, D. K.; Rabuck, A. D.; Raghavachari, K.; Foresman, J. B.; Ortiz, J. V.; Cui, Q.; Baboul, A. G.; Clifford, S.; Cioslowski, J.; Stefanov, B. B.; Liu, G.; Liashenko, A.; Piskorz, P.; Komaromi, I.; Martin, R. L.; Fox, D. J.; Keith, T.; Al-Laham, M. A.; Peng, C. Y.; Nanayakkara, A.; Challacombe, M.; Gill, P. M. W.; Johnson, B.; Chen, W.; Wong, M. W.; Gonzalez, C.; and Pople, J. A. *Gaussian 03*; Gaussian, Inc.: Pittsburgh, PA, 2003.
- (30) Reed, A. E.; Curtiss, L. A.; Weinhold, F. *Chem. Rev.* **1988**, 88, 899.

- (31) Hoffmann, M. M.; Darab, J. G.; Fulton, J. L. *J. Phys. Chem. A* **2001**, *105*, 1772.
- (32) Dolgos, M. R.; Paraskos, A. M.; Stoltzfus, M. W.; Yarnell, S. C.; Woodward, P. M. *J. Solid State Chem.* **2009**, *182*, 1964.
- (33) Mills, R. *J. Phys. Chem.* **1973**, *77*, 685.
- (34) Zhao, L.; Choi, P. *J. Chem. Phys.* **2004**, *120*, 1935.
- (35) Li, C.; Li, Z.; Choi, P. *Chem. Eng. Sci.* **2007**, *62*, 6709.